Experimental and theoretical investigation of CO oxidation on platinum: Bridging the pressure and materials gap

ARTICLE *in* PROCEEDINGS OF THE COMBUSTION INSTITUTE · JANUARY 2000

Impact Factor: 2.26 · DOI: 10.1016/S0082-0784(00)80348-3

6 AUTHORS, INCLUDING:

Frank Behrendt
Technische Universität Berlin
91 PUBLICATIONS **1,315** CITATIONS

Proceedings of the Combustion Institute, Volume 28, 2000/pp. 1341–1348

EXPERIMENTAL AND THEORETICAL INVESTIGATION OF CO OXIDATION ON PLATINUM: BRIDGING THE PRESSURE AND MATERIALS GAP

R. KISSEL-OSTERRIEDER,[1] F. BEHRENDT,[1] J. WARNATZ,[1] U. METKA,[2] H.-R. VOLPP[2] AND J. WOLFRUM[2]
[1]*Interdisziplinäres Zentrum für Wissenschaftliches Rechnen*
[2]*Physikalisch-Chemisches Institut*
Universität Heidelberg
Im Neuenheimer Feld 253, D-69120 Heidelberg, Germany

Optical IR-visible sum-frequency generation (SFG) surface vibrational spectroscopy was applied for *in situ* detection of chemisorbed CO during heterogeneous CO oxidation on a polycrystalline platinum catalyst. The substrate temperature was between 300 and 700 K at a total pressure of 20 mbar. Experiments were carried out under laminar flow conditions in a well-defined stagnation point flow geometry to allow for a detailed comparison with numerical reactive flow simulations. These were carried out to investigate the interaction among surface heterogeneity, catalytic surface reactions and gas-phase processes, and their coupling by molecular transport. To reproduce the experimental results, the model for the Pt foil is based on two different adsorption sites: ≈80% A and 20% B sites. The activation energy for desorption of a CO molecule on a clean surface was found to be 183 kJ/mol with a pre-exponential factor of $3 \cdot 10^{19}$ s^{-1} on the A sites and 220 kJ/mol with a pre-exponential factor of $5 \cdot 10^{21}$ s^{-1} on the B sites. A strong dependency of the desorption energy on the CO coverage was found on the A sites, dropping to 71 kJ/mol on a CO covered surface. These values match the heat of adsorption on Pt(111) and Pt(311) reported by King et al., suggesting structural similarities of these surfaces to a Pt foil. B sites were found to be effectively blocked in the presence of oxygen. But since no significant CO_2 production was observed at low temperatures, we conclude that B sites are not the active sites for the CO_2 formation. This finding could be explained by the strong bonding of oxygen to those sites.

Introduction

Catalytic steps contribute to approximately 90% of the production processes of industrial chemicals, fuels, and pharmaceuticals. In addition, catalysts are a key component in most approaches to the reduction of pollutants, such as those originating from combustion. Therefore, fundamental investigation of catalytic processes are a necessity.

The present paper demonstrates the bridging of the well-known pressure and materials gap between surface science and industrial catalysis, using carbon monoxide adsorption and its subsequent heterogeneous oxidation on platinum as an example. The reactions represent key steps of the overall reaction

$$2\ NO + 2\ CO \rightarrow N_2 + 2\ CO_2 \qquad (1)$$

which is one of the major pathways for the conversion of NO to N_2 in the automotive three-way catalytic converter [1]. Based on extensive ultrahigh vacuum (UHV) experiments on well-defined Pt single-crystal surfaces, it has been established that the reaction proceeds via a Langmuir–Hinshelwood mechanism where both reactants, CO and atomic oxygen, are adsorbed at the surface [2]. Although this single-crystal/UHV surface science approach has revealed detailed features of a variety of catalytic reactions [3], it was recognized quite early that it might not be possible to connect the chemistry identified on single crystals under UHV conditions ($p < 10^{-7}$ mbar) in a straightforward manner with real-life catalytic processes that usually take place at atmospheric pressure conditions (pressure gap) and on polycrystalline catalyst material (materials gap) [4].

The investigation of a polycrystalline Pt foil is a step toward a higher structural complexity of the catalyst surface and can be seen as an intermediate between single-crystal studies (see, for example, Refs. [5–9]) and investigations of nanoparticles on a washcoat used in industrial catalysis.

Recently, it was demonstrated that optical sum-frequency generation (SFG) spectroscopy could be a promising *in situ* diagnostics tool to bridge the pressure as well as the materials gap [10]. Using SFG, it was possible to monitor binding sites of CO surface species during high-pressure CO adsorption and catalytic CO oxidation on Pt(111) single-crystal model catalysts [11–13] as well as on polycrystalline Pt catalysts [14–17] up to atmospheric pressures.

In the present work, results are presented from a combined experimental and theoretical study of heterogeneous CO oxidation on a polycrystalline Pt catalyst at CO partial pressures of 2 mbar typically present in the exhaust gas of a spark-ignited engine. To

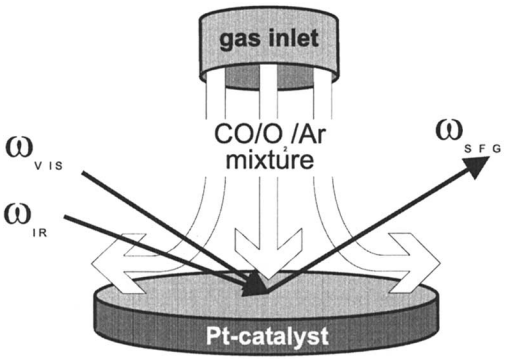

FIG. 1. Schematic description of the stagnation point flow geometry and the visible and IR laser beam alignment employed in the optical SFG experiments for the *in situ* detection of adsorbed CO species during catalytic CO oxidation under laminar flow conditions.

facilitate a detailed comparison between experiment and theory, the measurements were carried out in a reaction chamber, allowing for *in situ* SFG detection of CO at the surface during CO oxidation under laminar flow conditions in a well-defined stagnation-point flow geometry. For comparison with experimental results, numerical simulations of the reactive flow system corresponding to the conditions of the experiment were performed. The simulation is based on a computational model which includes detailed submodels for molecular transport and surface chemistry.

Experimental

The experiments were carried out in a reaction chamber, which allows catalytic studies starting from UHV conditions ($3 - 10^{-10}$ mbar) up to atmospheric pressure. In the high pressure regime, the experimental arrangement allows investigation of adsorption/desorption equilibrium and reactive processes for well-defined stagnation point flows of reactant mixtures on catalytic surfaces (Fig. 1) (for details see Ref. [17]). The reaction chamber was equipped with a quadruple mass spectrometer (QMS) for thermal-programmed desorption (TPD) measurements, an Ar^+ sputter source, a retarding field analyzer (RFA) for Auger electron spectroscopy (AES), and entrance and exit ports for the laser beams and the generated sumfrequency signal, respectively. A differentially pumped QMS was connected to the exhaust gas line behind the reaction chamber for online monitoring of the stable reaction product CO_2. The Pt catalyst (Pt foil, purity >99.99%) could be resistively heated in the temperature range 300–1600 K. Clean Pt surfaces were obtained by applying several cycles of Ar^+ ion sputtering followed by oxidation at 1000 K.

For the *in situ* detection of chemisorbed CO, a 40 ps mode-locked Nd:YAG laser system was used. A part of its output was frequency doubled to 532 nm and used as the visible input for the SFG process. The other part was used to pump an optical parametric system to generate IR radiation tunable in the frequency range of 1800–2200 cm^{-1} [13]. The visible and the IR laser beams were *p*-polarized and overlapped at the surface (see Fig. 1). The CO sum-frequency signal reflected from the Pt surface was detected by a photomultiplier and a gated integrator and transferred to a laboratory computer. The principles of SFG surface vibrational spectroscopy have been described in detail elsewhere [18]. SFG is a second-order nonlinear optical process where a tunable infrared (ω_{IR}) laser beam is mixed with a visible (ω_{VIS}) laser beam to generate a sum-frequency output (ω_{SFG}). Because in the electric dipole approximation this process is only allowed in a medium without centrosymmetry for the CO gas-phase/Pt system, the SFG signal is highly specific to the interface region bounded by the centrosymmetric media. In the SFG experiment, the visible beam is held at a fixed frequency while the IR beam is tuned over the vibrational range of interest. When the IR beam is tuned over a vibrational resonance of a surface species, the effective surface nonlinear susceptibility is resonantly enhanced. Because the SFG intensity is proportional to the absolute square of the effective surface nonlinear susceptibility, a vibrational spectrum of the surface species can be measured. Details about the simulation of SFG spectra measured for the CO/Pt foil system are given in Refs. [13,17].

Model

Governing Equations and Boundary Conditions

The simulation is based on the model of a reactive stagnation-point flow directed toward a reactive surface. The integration domain covers the region between the gas inlet and the substrate (see Fig. 1). The variables (density, momentum, temperature, and mass fraction of each gas-phase species; special care is taken with the radial pressure gradient) are independent of radius and depend only on the distance from the surface. This system is closed by the ideal gas law. The boundary-value problem that has to be solved has been stated by Evans and Greif [19] and by Kee et al. [20].

The solution of the gas-phase problem is coupled with the surface properties and reaction mechanism. In a mean-field (MF) model, the surface state is described by averaged surface coverages of the adsorbates. The temporal development of the coverages is calculated from macroscopic surface reaction rates. Adsorbate–adsorbate interactions are replaced by averaged values, assuming a randomly distributed

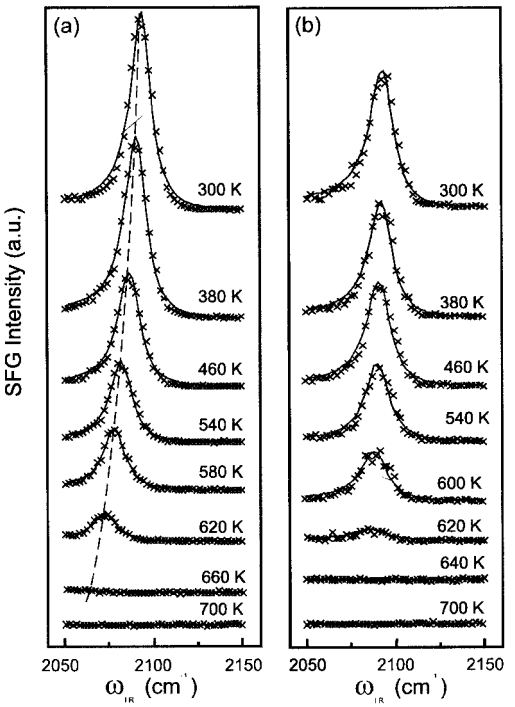

FIG. 2. (a) SFG C–O stretching vibrational spectra of CO terminally adsorbed on a polycrystalline Pt foil. The SFG signal intensity is plotted versus the frequency (ω_{IR}) of the tunable IR laser. The spectra were recorded under CO adsorption/desorption equilibrium conditions at a CO pressure of 1 mbar. (b) SFG spectra measured during the heterogeneous CO oxidation at different substrate temperatures at a total pressure of 20 mbar. Measurements were performed under laminar flow conditions in a stagnation point flow (CO, 15 sccm; O_2, 30 sccm; Ar, 105 sccm). The dashed line in Fig 2a indicates the pronounced spectral shift from 2096 cm^{-1} at 300 K to 2057 cm^{-1} at 660 K which does not occur in the experiments of Fig 2b. Crosses represent experimental data (every data point was obtained by averaging more than 120 laser shots at a laser repetition rate of 10 Hz); solid lines are the results of simulations of the SFG line shapes carried out to derive the CO vibrational frequencies (for details see Ref. [13]).

adlayer. A detailed discussion of the governing equations, boundary conditions, and transport model can be found in Ref. [21].

The Navier–Stokes equations describing the gas phase together with the boundary conditions represent a differential–algebraic equation system. To solve this, a finite difference discretization scheme using a statically adapted non-equidistant grid is applied. The resulting system of ordinary differential equations is solved using the extrapolation solver LIMEX [22,23].

Sensitivity Analysis

A key step in improving detailed reaction mechanisms is the application of a sensitivity analysis. This technique has been proven to be very useful in understanding homogeneous combustion processes. It allows identification of those elementary reaction steps that are most influential to the system. This identification acts as a guidance for further experimental work aiming toward improved kinetic data.

In order to derive the governing equations for the sensitivity coefficients, let us start from the system of differential and algebraic equations, which results after spatial discretization of the governing system of partial differential equations

$$\frac{\partial \mathbf{y}}{\partial t} = \mathbf{F}(\mathbf{y}) \tag{2}$$

where $\mathbf{y}$ is the n-dimensional vector of the dependent variables at the surface, the gas phase, and at the outer boundary, and $\mathbf{F}$ is a vector valued function of these variables. Differentiation with respect to the n_p parameters p_i leads to

$$\frac{\partial}{\partial p_i}\frac{\partial \mathbf{y}}{\partial t} = \frac{\partial}{\partial p_i}\mathbf{F}(\mathbf{y}) \tag{3}$$

Defining $s_i = \partial \mathbf{y}/\partial p_i$ as the sensitivity coefficient with respect to parameter p_i, we obtain

$$\frac{\partial s_i}{\partial t} = \mathbf{F}_{\mathbf{y}} s_i + \mathbf{F}_{\mathbf{p}_i} \tag{4}$$

where $\mathbf{F}_{\mathbf{y}}$ denotes the Jacobian matrix of the system ($\mathbf{F}_{y_{j,k}} = \partial \mathbf{F}_j/\partial \mathbf{y}_k$) and $\mathbf{F}_{\mathbf{p}_i}$ the vector of partial derivatives of $\mathbf{F}$ with respect to the parameter p_i. (Note that in the stationary case this formulation is equivalent to the sensitivity equations of the stationary problem.) Thus, a linear ordinary differential equation system for the sensitivity coefficients is obtained, which is solved together with the solution of the system equations.

Results and Discussion

CO Adsorption/Desorption Equilibria

Recently, CO adsorption on polycrystalline Pt was studied over a wide pressure range at room temperature. The present work is aimed at the investigation of the temperature dependence of the CO adsorption on a polycrystalline Pt foil. Therefore, SFG spectra of adsorbed CO were measured in the temperature range T = 300–660 K at a CO pressure of 1 mbar under adsorption/desorption equilibrium conditions (see Fig. 2a). Solid lines in Fig. 2a are results of simulations of the SFG line shape carried out to derive the maximum value of the resonant part of the SFG intensity, I_{SFG} (ω_{CO}), and the CO

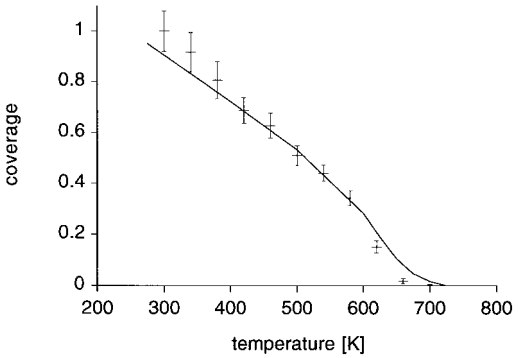

FIG. 3. CO surface coverage (bars) as a function of the Pt substrate temperature measured under CO adsorption/desorption equilibrium conditions at a constant CO gas-phase pressure of 1 mbar. The initial value represents the saturation coverage of the polycrystalline Pt surface at T = 300 K. The symbol at T = 700 K indicates zero coverage. The solid line is the result of a numerical simulation assuming two different CO adsorption sites and a stagnation-point flow of CO onto the Pt foil corresponding to the conditions of the experiment. Details of the surface adsorption model are given in the text.

vibrational frequency, ω_{CO}. Detailed calibration experiments under UHV conditions in which the SFG method was combined with TPD measurements for the direct CO surface coverage determination revealed that for the CO/Pt foil system the SFG intensity at the resonance frequency I_{SFG} (ω_{CO}) is the spectroscopic quantity which correlates linearly with CO surface coverage [16]. CO coverages derived from the SFG measurements are plotted in Fig. 3 against the Pt substrate temperature. The CO coverage versus substrate temperature plot shown in Fig. 3 clearly indicates the presence of two different adsorption/desorption regimes, one in the temperature range 300 K $< T <$ 580 K in which the equilibrium coverage decreases almost linearly with substrate temperature, and a second one at $T >$ 600 K in which the equilibrium coverage decreases more rapidly with increasing substrate temperature. This behavior indicates the presence of at least two distinct CO adsorption sites on the Pt foil with markedly different activation energies for desorption. More details about the nature of these adsorption sites in the CO/Pt foil system can be obtained from an analysis of the temperature and coverage dependence of the measured CO vibrational frequencies and a comparison with the results of SFG and IR reflection–absorption spectroscopy (IRAS) experiments on different Pt single crystal surfaces [24–26]. SFG studies on a Pt(111) single crystal at T = 300 K yielded a value of ω_{CO} = 2093.3 ± 1.6 cm^{-1} at saturation coverage. In Ref. [25], a comparable value of ω_{CO} = 2097 cm^{-1} was reported for the high coverage limit on a Pt[4(111) × (100)] surface. In both cases, the frequency was assigned to CO terminally bonded on (111) terrace-site Pt atoms. Within the experimental uncertainty, the value of ω_{CO} = 2096 ± 4 cm^{-1} observed in present study at T = 300 K is in good agreement with these values, indicating the presence of (111) terraces on the Pt foil. In the low coverage regime (below 40% of saturation coverage), resonance frequencies in the range ω_{CO} = 2065–2078 cm^{-1} were determined in IRAS studies on the Pt[4(111) × (100)] surface and were assigned to CO terminally bonded on step-site Pt atoms [25]. These frequency values as well as their CO coverage dependence are in agreement with the results of the present study, indicating similarity in the topology of the Pt[4(111) × (100)] and the polycrystalline Pt foil surface. This interpretation is further supported by TPD studies, which revealed a close similarity in the (111) terrace/step-site structure between the Pt[4(111) × (100)] and polycrystalline Pt surfaces [25,27]. The Pt[4(111) × (100)] surface consists of (111) terraces which are four atoms wide, separated by monatomic straight steps with 25% of its exposed atoms coordinated to seven nearest neighbors [compared to nine neighbors for the remaining (111) terrace-site Pt atoms]. In the light of the above described similarity between the polycrystalline and the Pt[4(111) × (100)] surface topology, a surface reaction model was developed which accounts for two distinct Pt atom adsorption sites (A and B) based on surface kinetics data obtained on Pt(111) (for the A sites) and on single-crystal surfaces exhibiting seven-fold coordinated CO adsorption sites (for the B sites). The solid line in Fig. 3 represents results of a numerical simulation in which a value of 183 kJ/mol for the activation energy for desorption (together with a pre-exponential factor of $3 \cdot 10^{19}$ s^{-1}) was assigned to the A sites, while for the more strongly bound B sites an activation energy of 220 kJ/mol (together with a pre-exponential factor of $5 \cdot 10^{21}$ s^{-1}) was used. For the CO sticking probability, the Kisliuk model [28] with an initial sticking probability of 0.7 at T = 300 K was applied. In the model, it was assumed that the surface consists of 80% A sites and 20% B sites. This ratio of sites is supported by TPD spectra observed at the used Pt foil. For the A sites, a strong dependence of the activation energy for desorption was observed, with the value decreasing from 183 kJ/mol for an isolated molecule to 71 kJ/mol for the initial coverage. For the B sites, a more moderate decrease of 14 kJ/mol was found. The A-site activation energy value used in the simulation is in good agreement with the initial heat of adsorption value of 187 ± 11 kJ/mol [29] determined by King and co-workers for Pt(111). The latter measurements also revealed a coverage dependency of the adsorption heat, with a moderate decrease for coverages below 0.5 ML followed by a sharp decrease at higher coverages. The B-site activation energy value closely matches the initial heat

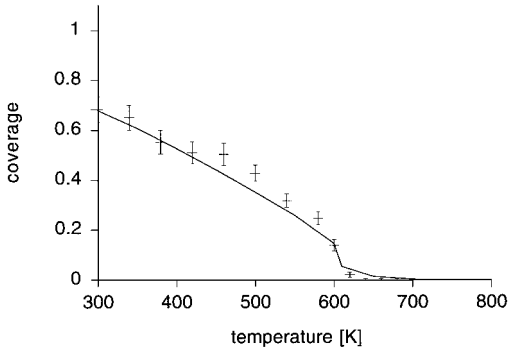

FIG. 4. CO surface coverage (bars) as a function of the Pt substrate temperature measured during CO oxidation at a pressure of 20 mbar. Measurements were carried out under laminar flow conditions in a stagnation point flow (CO, 15 sccm; O_2, 30 sccm; Ar, 105 sccm). The solid line is the result of a numerical simulation corresponding to the conditions of the experiment. Details of the surface reaction model are given in the text.

of adsorption of 210 ± 7 kJ/mol which was recently determined by King and co-workers for the Pt(311) surface for which CO adsorption occurs predominately at seven-fold coordinated Pt atoms located on sites [30]. In this study, a moderate decrease of the initial heat of adsorption to a value of 190 ± 6 kJ/mol was observed in the coverage range of 0.1–0.8 ML (monolayer).

CO Oxidation

The SFG spectra shown in Fig. 2b which were recorded during CO oxidation (CO, 15 sccm; O_2, 30 sccm; Ar, 105 sccm; total pressure, 20 mbar) were evaluated in order to determine I_{SFG} (ω_{CO}) and hence the CO coverage as a function of substrate temperature, as depicted in Fig. 4. Comparison with the CO coverage measured during the CO adsorption/desorption studies (Fig. 3) reveals that if O_2 is present in the stagnation flow, the CO coverage at $T = 300$ K is considerably reduced. However, although the total CO surface coverage is reduced by about 30%, the CO vibrational frequency remains at a value of 2095 ± 4 cm^{-1} typical for the saturation coverage vibrational frequency of CO terminally adsorbed at Pt(111) terrace sites (A sites) [24]. In addition, in contrast to the observation in the CO adsorption study, during CO oxidation over the whole temperature range where chemisorbed CO could be detected, the CO vibrational frequency remains in the range 2095–2078 cm^{-1}. Hence, the striking difference between the CO adsorption/desorption and the present CO oxidation data is the absence of the low-frequency CO contribution from step sites (denoted as B sites in the previous section) in the latter case. This could be explained by a higher sticking probability of O_2 at the step sites which efficiently blocks CO step-site adsorption when both CO and O_2 are present in the gas phase. Such a preferential adsorption of O_2 on step sites has been observed in electron-stimulated desorption ion angular distribution (ESDIAD) studies on Pt[3(111) × (100)] [31] and during IRAS studies of CO oxidation on Pt[4(111) × (100)] [32]. In Fig. 4, the results of a numerical simulation are compared with the experimental results. The simulation is based on the well-established Langmuir–Hinshelwood (LH) scheme for CO oxidation, including adsorption and desorption of CO (as described in the previous section) and oxygen as well as the formation of CO_2 through reaction of the adsorbed CO and O species [2]. The corresponding surface reaction mechanism is summarized in Table 1. Although the results of the numerical simulation shown in Fig. 4, with the two different coverage versus temperature regimes, look similar to the one shown in Fig. 3, the origins of these particular curve shapes are quite different. During CO oxidation, the sudden decrease observed at higher temperatures does not result from the difference in the desorption kinetics of the A and B sites, as in the present model B sites are actually blocked by oxygen. The rapid decrease of the CO coverage on the A sites at $T > 600$ K is due to a transition from a CO-covered to an O-covered state initiated through an increase of oxygen adsorption with decreasing CO coverage and the increase of the LH reaction rate. A comparison between the measured and the calculated CO_2 production rate is shown in Fig. 5.

Figure 6 shows results of a sensitivity analysis of the A-site CO coverage. Of course, the parameters for CO adsorption/desorption, which are already fixed by the CO adsorption/desorption measurements, have a strong impact on the A-site CO coverage. In addition, increasing the oxygen sticking probability on A sites would lead to a decrease of the A-site CO coverage. In the model, it was assumed that the oxygen sticking probability depends on the actual CO coverage, dropping quickly from an initial value of 0.05 to about 2% of this value at a CO coverage of 0.5. This assumption is supported by experimental investigations [2] and can be explained by the reduced availability of adjacent free sites for the oxygen adsorption as a result of the repulsive interaction between CO adsorbate molecules [33].

With increasing temperature, the absolute values of the sensitivity coefficients increase up to a temperature of 600 K. At this temperature, the transition to the predominantly oxygen covered state occurs. With further increasing temperature, the absolute values of the sensitivity coefficients rapidly decrease again. This behavior is typical for a system which undergoes a transition from a poisoned, nonreactive state, which is predominantly determined

TABLE 1
Surface reaction mechanism for the oxidation of CO on a Pt foil

Reaction	v (cm^2 mol s)	E_0 (kJ/mol)	E_1 (kJ/mol)	S_0	Ref.
A sites					
O_2 ads				0.05	[35]
O_2 des	$3.7 \cdot 10^{21}$	210.0			[36]
CO ads				0.75	[29]
CO des	$3.0 \cdot 10^{19}$	183.0	71.0		This work
CO_2 prod	$6.0 \cdot 10^{21}$	90.0			This work
B sites					
O_2 ads				$\simeq 1$	This work
CO ads	In the absence of oxygen			0.75	This work
CO ads	In the presence of oxygen			≤ 0.10	This work
CO des	$5.0 \cdot 10^{21}$	220.0	206.0		This work
A and B-site combinations					
CO_2 prod	$6.0 \cdot 10^{21}$	105.0			This work

Note: Parameters on the A sites referred to the literature are for Pt(111). E_0 and E_1 are the activation energies for an isolated molecule and for a molecule at saturation coverage for $p_{CO} = 1$ mbar and 300 K; ads, adsorption; des, desorption; prod, production.

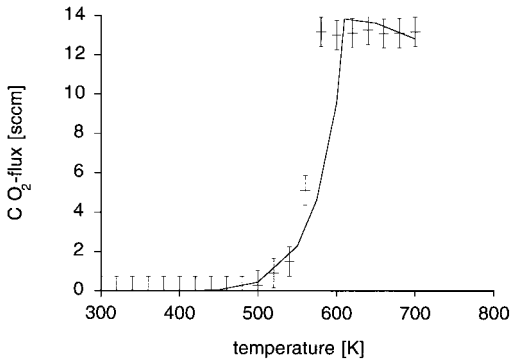

FIG. 5. Comparison between the measured (bars) and the calculated (solid line) CO_2 production rate. Measurements were carried out under laminar flow conditions in a stagnation-point flow onto the Pt foil (CO, 15 sccm; O_2, 30 sccm; Ar, 105 sccm). Ar served as an inert buffer gas and as an internal standard for the mass spectrometric determination of the absolute CO_2 production rate. Complete conversion of CO to CO_2 would result in a CO_2 flow rate of 15 sccm. The height of the bars represent the systematic uncertainty in the CO_2 production rate measurements due to the presence of a small CO_2 background signal which was observed in the exhaust line of the reaction chamber already at room temperature. The solid line is the result of a numerical simulation corresponding to the conditions of the experiment. Details of the surface reaction model are given in the text.

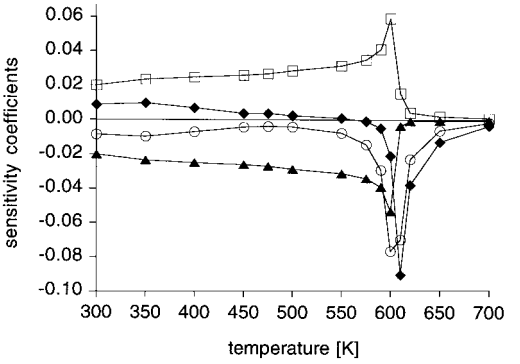

FIG. 6. Sensitivity analysis of the A-site CO coverage with respect to the rate parameter of the most relevant elementary reactions. Open circles, adsorption of oxygen; open squares, adsorption of CO; filled triangles, desorption of CO; filled diamonds, LH reaction. All elementary steps are referred to reactions at A sites. Reactions on B sites and A and B combinations are of minor importance.

by the chemical reactions, to a reactive state, which is predominantly controlled by transport limitations in the gas phase. This is also reflected in steep gradients of the gas-phase species profiles obtained numerically.

Assuming a LH scheme also for the B sites, the oxygen-covered state can only be stabilized down to 300 K, if the activation energy of the LH reaction is only half as high as on the A sites. Consequently, this would lead to a high CO_2 production rate also at low temperatures. As clearly can be seen from sensitivity

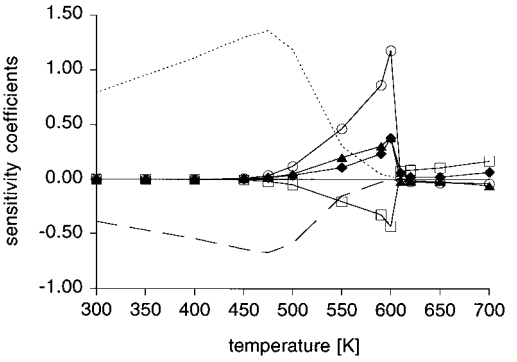

FIG. 7. Sensitivity analysis of the CO_2 production rate with respect to the rate parameter of the most relevant elementary reactions. Referred to reactions at A sites: open circles, adsorption of oxygen; open squares, adsorption of CO; filled triangles, desorption of CO; filled diamonds, LH reaction. Referred to reactions at B sites: dotted line, adsorption of CO; dashed line, adsorption of oxygen.

analysis (see Fig. 7), the CO sticking probability on B sites then is the rate-limiting step for the CO_2 production at low temperatures. Oxygen adsorption on B sites also considerably influences the CO_2 production rate at low temperatures. An increase of the oxygen sticking probability on the B sites would cause a decrease of the CO_2 production rate, which again reflects the fact that CO adsorption, competing with oxygen adsorption, is rate limiting. Since only negligibly low CO_2 production is observed experimentally (see Fig. 5), we conclude that oxygen efficiently blocks CO adsorption on B sites and that therefore these sites are not the active sites for CO_2 production. On the other hand, since oxygen on B sites can react with CO on A sites, the presence of B sites destabilizes the CO-poisoned state on the A sites. The LH reaction rate at A and B site combinations influences the temperature where the transition to the oxygen covered state on the A sites occurs. Furthermore, B sites could act as nucleation centers for the transition to the oxygen covered state and thus increase the overall reactivity of the surface. This effect of oxygen-type defects has been reported by Berdau et al. [34] and can be reproduced by Monte Carlo calculations [33].

Conclusions

In the present study, SFG surface vibrational spectroscopy of adsorbed CO species was combined with detailed numerical simulation and sensitivity analysis to investigate the heterogeneous CO oxidation on a polycrystalline Pt catalyst under laminar flow conditions at millibar reactant pressures. A detailed surface reaction mechanism based on UHV surface kinetics data was developed which takes into account the surface heterogeneity of the polycrystalline catalyst. With this model, the experimental results could be successfully described, indicating that for the CO/O_2 Pt foil system, UHV surface kinetics data obtained on well-defined small-area Pt single crystals can reproduce the catalytic behavior of the more realistic polycrystalline catalyst for intermediate CO reactant pressures as typically present in the exhaust gas of spark-ignited engines. Extension of the present work toward detailed experimental and theoretical investigations of NO adsorption/dissociation steps and the subsequent reaction processes with CO on different catalyst materials under typical three-way catalyst reactant pressure conditions is planned for the near future.

Acknowledgments

This work was supported by the Deutsche Forschungsgemeinschaft within the Sonderforschungsbereich 359, Reaktive Strömungen, Diffusion und Transport.

REFERENCES

1. Fink, Th., Dath, J.-P., Bassett, M. R., Imbihl, R., and Ertl, G., *Surf. Sci.* 245:96 (1991).
2. Engel, T., and Ertl, G., *Adv. Catal.* 28:1 (1979).
3. Ertl, G., in *Catalysis Science and Technology 4,* (J. R. Anderson and M. Boudart, eds.) Springer, New York, 1983 p. 209; Somorjai, G. A., *Introduction to Surface Chemistry and Catalysis,* John Wiley and Sons, New York, 1994, and references therein.
4. Somorjai, G. A., *Appl. Surf. Sci.* 121–122:1 (1997), and references therein.
5. Berdau, M., Yelenin, G. G., Karpowicz, A., Ehsasi, M., Christmann, K., and Block, H., *J. Chem. Phys.* 110 (23):11551 (1999).
6. Wintterlin, J., Völkening, S., Janssens, T. V. W., Zambelli, T., and Ertl, G., *Science* 278:1931 (1997).
7. Xu, M., Liu, J., and Zaera, F., *J. Chem. Phys.* 104:8825 (1996).
8. Rotermund, H. H., *Surf. Sci.* 386:10 (1997).
9. Jakubith, S., Rotermund, H. H., Engel, W., von Oertzen, A., and Ertl, G., *Phys. Rev. Lett.* 65:3013 (1990).
10. Somorjai, G. A., and Rupprechter, G. J., *Phys. Chem. B* 103:1623 (1999), and references therein.
11. Su, X., Cremer, P. S., Shen, Y. R., and Somorjai, G. A., *Phys. Rev. Lett.* 77:3858 (1996).
12. Su, X., Cremer, P. S., Shen, Y. R., and Somorjai, G. A., *J. Am. Chem. Soc.* 119:3994 (1997).
13. Härle, H., Mendel, K., Metka, U., Volpp, H.-R., Willms, L., and Wolfrum, J., *Chem. Phys. Lett.* 279:275 (1997).
14. Wolfrum, J., *Proc. Combust. Inst.* 27:1–41 (1998).
15. Härle, H., Lehnert, A., Metka, U., Volpp, H.-R., Willms, L., and Wolfrum, J., *Chem. Phys. Lett.* 293:26 (1998).

16. Härle, H., Lehnert, A., Metka, U., Volpp, H.-R., Willms, L., and Wolfrum, J., *Appl. Phys. B* 68(3):567 (1999).
17. Härle, H., Metka, U., Volpp, H.-R., and Wolfrum, J., *Phys. Chem. Chem. Phys.* 1:50–59 (1999).
18. Shen, Y. R., *Nature* 337:519 (1989), and references therein.
19. Evans, G. H., and Greif, R., *ASME J. Heat Transfer* 109:928 (1987).
20. Kee, R. J., Miller, J. A., Evans, G. H., and Dixon-Lewis, G., *Proc. Combust. Inst.* 22:1479–1494 (1988).
21. Deutschmann, O., Behrendt, F., and Warnatz, J., *Catal. Today* 46:155–163 (1998).
22. Deuflhard, P., Hairer, E., and Zugck, J., *Num. Math.* 51:501 (1987).
23. Deuflhard, P., and Nowak, U., "Large Scale Scientific Computing," in *Progress in Scientific Computing Vol. 7* (P. Deuflhard, B. Enquist, eds.), Birkhaeuser, Boston, 1987, p. 37.
24. Klünker, C., Balden, M., Lehwald, S., and Daum, W., *Surf. Sci.* 360:104 (1996).
25. Hayden, B. E., Kretzschmar, K., Bradshaw, A. M., and Greenler, R. G., *Surf. Sci.* 149:394 (1985).
26. Xu, J., Yates Jr., J. T., *Surf. Sci.* 327:193 (1995).
27. Levoguer, C. L., and Nix, R. M., *Surf. Sci.* 365:672 (1996).
28. Kisliuk, P., *J. Phys. Chem. Solids* 3:95 (1954).
29. Brown, W. A., Kose, R., and King, D. A., *Chem Rev.* 98:797–832 (1998).
30. Kose, R., and King, D. A., *Chem. Phys. Lett.* 313:1–6 (1999).
31. Szab, A., Henderson, M. A., and Yates Jr., J. T., *J. Chem. Phys.* 96:6191 (1992).
32. Xu, J., and Yates Jr., J. T., *J. Chem. Phys.* 99:725 (1993).
33. Kissel-Osterrieder, R., Behrendt, F., and Warnatz, J., *Proc. Combust. Inst.* 28:1323–1330 (2000).
34. Berdau, M., Yelenin, G. G., Karpowicz, A., Ehsasi, M., Christmann, K., and Block, H., *J. Chem. Phys.* 110:11551–11573 (1999).
35. Winkler, A., Guo, X., Siddiqui, H. R., Hagans, P. L., and Yates Jr., J. T., *Surf. Sci.* 201:419–443 (1988).
36. Parker, D. H., Bartram, M. E., and Koel, B. E., *Surf. Sci.* 217:489–510 (1989).

COMMENTS

K.-H. Homann, Technische Universität Darmstadt, Germany. How do you calibrate for the CO range of the Pt foil?

Author's Reply. In order to derive CO surface coverage from the measured SFG spectra, calibration measurements were carried out in which SFG detection of CO was combined with thermal desorption measurements of CO. A detailed description of the calibration procedure can be found in Ref. [1]:

REFERENCE

1. Härle, H., Lehnert, A., Metka, U., Volpp, H.-R., Williams, L., and Wolfrum, J., *Appl. Phys.* B 68/3:567 (1999).

•

D. G. Vlachos, University of Delaware, USA. Are you able to deconvolute the shift in vibrational frequency with coverage? Can you detect the effect of gas-phase composition on the activation energy of surface reaction?

Author's Reply. The dependence of the CO vibrational frequency on the CO coverage could be determined by analyzing SFG spectra obtained for different CO surface coverages employing a numerical simulation of the vibrational resonant contribution of the spectra [1]. For the polycrystalline foil used in the present work, we found a coverage dependence of the CO vibrational frequency similar to that observed for a sputtered Pt (111) single crystal surfaces [2,3]. The CO oxidation studies were carried out for a fixed CO/O_2 gas-phase composition ($pCO = 2$ mbar, $pO_2 = 4$ mbar). In the present studies, no attempts were made to investigate the effect of different gas-phase compositions on the activation energy of the surface reaction.

REFERENCES

1. Härle, H., Lehnert, A., Metka, U., Volpp, H.-R., Willms, L., and Wolfrum, J., *Chem. Phys. Lett.* 293:26 (1998).
2. Klünker, C., Balden, M., Lehwald, S., Daum, W., *Surf. Sci.* 360:104 (1996).
3. Härle, H., Mendel, K., Metka, U., Volpp, H.-R., Williams, L., and Wolfrum, J., *Chem. Phys. Lett.* 279:275 (1997).